J. Anat. (2007) **210**, pp272–293 doi: 10.1111/j.1469-7580.2007.00696.x

Ontogenetic relationships between *in vivo* strain environment, bone histomorphometry and growth in the goat radius

Russell P. Main

Concord Field Station, Department of Organismic and Evolutionary Biology, Harvard University, USA

Abstract

Vertebrate long bone form, at both the gross and the microstructural level, is the result of many interrelated influences. One factor that is considered to have a significant effect on bone form is the mechanical environment experienced by the bone during growth. The work presented here examines the possible relationships between *in vivo* bone strains, bone geometry and histomorphology in the radii of three age/size groups of domestic goats. *In vivo* bone strain data were collected from the radii of galloping goats, and the regional cortical distribution of peak axial strain magnitudes, radial and circumferential strain gradients, and longitudinal strain rates related to regional patterns in cortical growth, porosity, remodelling and collagen fibre orientation. Although porosity and remodelling decreased and increased with age, respectively, these features showed no significant regional differences and did not correspond to regional patterns in the mechanical environment. Thicker regions of the radius's cortex were significantly related to high strain levels and higher rates of periosteal, but not endosteal, growth. However, cortical growth and strain environment were not significantly related. Collagen fibre orientation varied regionally, with a higher percentage of transverse fibres in the caudal region of the radius and primarily longitudinal fibres elsewhere, and, although consistent through growth, also did not generally correspond to regional strain patterns. Although strain magnitudes increased during ontogeny and regional strain patterns were variable over the course of a stride, mean regional strain patterns were generally consistent with growth, suggesting that regional growth patterns and histomorphology, in combination with external loads, may play some role in producing a relatively 'predictable' strain environment within the radius. It is further hypothesized that the absence of correlation between regional histomorphometric patterns and the measured strain environments is the result of the variable mechanical environment. However, the potential effects of other physiological and mechanical factors, such as skeletal metabolism and adjacent muscle insertions, that can influence the gross and microstructural morphology of the radius during ontogeny, cannot be ignored.

Key words bone histology; bone strain; bone; collagen; CPL; growth; ontogeny; remodelling.

Introduction

Many factors influence long bone morphology in the vertebrate skeleton. These factors are interrelated and include mechanical, hormonal, environmental, nutritional and phylogenetic influences (Horner et al. 2000; Lee & Lanyon, 2004). From a mechanical point of view, vertebrate limb bones grow (model) and alter their shape and structure (remodel) to obtain and maintain rigid support structures capable of resisting the mechanical forces placed upon them. During growth, resistance to loading within the limb bones is primarily the product of ontogenetic increases in the size of the bones, which results in more bone material available to resist mechanical deformation, and ontogenetic changes in the material properties of the bone tissue itself, which results in an increased elastic modulus (Carrier, 1983; Currey & Pond, 1989; Brear et al. 1990) and, thus, a

Correspondence
Dr Russell P. Main, Concord Field Station, Department of Organismic and Evolutionary Biology, Harvard University, 100 Old Causeway Road, Bedford, MA 01730, USA. E: rmain@oeb.harvard.edu

Accepted for publication *28 November 2006*

stiffer bone element. Additionally, bone remodelling helps to maintain a bone's resistance to loading throughout an animal's life by replacing bone tissue that may have become damaged during previous loading events. In both cancellous and cortical bone, remodelling can also result in bone tissue that is more closely aligned with prevailing force trajectories (Wolff, 1892; Carter et al. 1989; Riggs et al. 1993a,b; Biewener et al. 1996; Pontzer et al. 2006; but see Bertram & Swartz, 1991), potentially even acting in regionally specific ways to differentially affect parts of the bone experiencing different mechanical environments (Riggs et al. 1993a,b; Mason et al. 1995).

Relationships between bone geometry and loading

Functional interpretations of long bone morphology, without prior knowledge of the loading environment, often rely on mechanical beam theory. In this approach, it is often assumed that modelling and remodelling act to minimize the deformations (strains) due to load, to maintain a high factor of safety within the bone (see Lanyon, 1987). Thus, when bending loads are assumed, which are common in terrestrial vertebrate long bones (Rubin & Lanyon, 1982; Biewener, 1991), it is hypothesized that the bones are loaded most frequently or under the greatest forces across the axis about which the majority of the bone tissue is distributed, coinciding with the maximum second moment of area. These hypotheses are supported by studies that have experimentally increased bending loads upon the limb bones and shown that new bone growth and/or remodelling occur where the induced strains are greatest (Robling et al. 2001; Mosley & Lanyon, 2002), thereby increasing the amount of bone material available to resist these loads. These modelling responses by the bone can result in a decrease in the induced strains over time (Goodship et al. 1979; Lanyon et al. 1982).

However, it is also argued that bones require a certain strain stimulus to maintain bone mass, suggesting that the minimization of strains may not be the driving force behind bone modelling and remodelling. During prolonged decreases in functional loading in adult animals, bone resorption can outpace bone growth, resulting in a net decrease in bone tissue (Rubin et al. 1996; Vico et al. 2000). Consistent with previous theories (Frost, 1983; Beaupré et al. 1990; van der Meulen et al. 1993), recent studies examining the effects of induced loads of varying magnitude upon the limbs have shown that there is a certain minimum stress or strain threshold required for bone maintenance and the growth of bone tissue (Mosley et al. 1997; Hsieh et al. 2001). However, a modelling/remodelling balance must be achieved that allows for the required strain stimulus during typical loading, but still preserves a sufficient safety factor to withstand atypical or unexpected loads when they occur.

Recognizing the need for this balance, previous workers have hypothesized that bone modelling and remodelling may act, if not to minimize strains within the bone, to direct them in a more predictable fashion (Lanyon, 1987; Bertram & Biewener, 1988). Improved loading predictability of limb bones can result from eccentric cross-sectional bone shape, longitudinal curvature and/or muscle action within the limbs (Pauwels, 1980; Lanyon, 1987; Bertram & Biewener, 1988) and has been supported by *in vivo* studies showing that, in a variety of terrestrial vertebrates (primarily mammals), maximum longitudinal bending within the bones often acts across the minimum second moment of area (Lanyon et al. 1982; Rubin & Lanyon, 1982, 1985; Biewener, 1991; Judex et al. 1997; Demes et al. 1998; Lieberman et al. 2003). Although loading in this direction would not minimize bone strains, asymmetric bone morphology should make the direction of loading more predictable by predisposing the bone to be consistently bent in a particular direction (Lanyon, 1987; Bertram & Biewener, 1988). In these cases, the *in vivo* direction of bending contrasts with predictions based upon the functional application of engineering beam theory.

When *in vivo* strain recordings from three locations about a bone have been used to determine the normal (longitudinal) strain environment throughout the entire cross-section of a bone, the strain distributions reported during the time of peak strains, even for asymmetrical cross-sectional shapes, do not necessarily coincide with either the minimum or the maximum second moments of area, but often fall somewhere in between (Gross et al. 1992; Biewener & Dial, 1995; Demes et al. 2001; Lieberman et al. 2004; Main & Biewener, 2004). This is at odds with hypotheses that adult bone form results strictly from selection for either minimizing peak bone strains or making strains more predictable. However, such intermediate strain distributions may reflect a compromise between strain levels that are great enough to stimulate growth and maintain bone mass while still protecting against possible unexpected loading events.

Relationships between bone histomorphometry and loading

Attempts have also been made at predicting or relating the loading of long bones to their microstructural architecture. Following from work examining relationships between cancellous and whole bone morphology and functional loading, it is reasonable to expect that elements within the cortical bone microstructure should also respond to prevailing strain environments within the bone. Two aspects that have been examined previously in relation to functional strain environments are regional patterns of remodelling and collagen fibre orientation (Riggs et al. 1993a,b; Mason et al. 1995; Rubin et al. 1996; de Margerie, 2002; Skedros et al. 2003; Lee, 2004; de Margerie et al. 2005).

Remodelling within cortical bone can occur for at least two reasons: (1) to replace mechanical damage and (2) to access bone mineral for metabolic needs (Currey, 2002; Martin, 2002). Greater amounts of bone remodelling coincide with increased bone microdamage in bones experimentally subjected to increased strain frequencies and/or magnitudes (Burr et al. 1985; Bentolila et al. 1998; Lee et al. 2002; Lieberman et al. 2003), indicating a link between high strain environments and remodelling. However, when remodelling occurs in either trabecular or cortical bone for metabolic reasons, it might be expected that bone mineral would be resorbed where a decrease in structural support would have the least mechanical effect (i.e. where strains are lowest). However, the possible regionalization of remodelling for reasons other than damage repair has not been investigated explicitly (Parfitt, 2002).

Collagen fibre orientation (CFO) could also be a potential indicator of strain environments within cortical bone, reflecting the potential for bone's microstructure to become better aligned mechanically through bone remodelling. Results from mechanical tests of cortical bone have shown that bone composed primarily of longitudinal collagen fibres is stronger in tension than bone composed primarily of transverse or oblique fibres, which is stronger in compression and shear (Evans & Vincentelli, 1969, 1974; Vincentelli & Evans, 1971). Although a number of studies generally support a correlation between *in vivo* strain patterns and CFO (horse radius and bird limb bones; Riggs et al. 1993a,b; Mason et al. 1995; de Margerie et al. 2005), others have reported inconsistent results (sheep calcaneus and alligator femur; McMahon et al. 1995; Lee, 2004).

In many of these previous studies investigating relationships between cortical growth, porosity, remodelling, CFO and *in vivo* bone strains, mechanical and histomorphological data were not collected from the same individual animals, leaving potential intra- or interspecific variations in functional strain patterns unaccounted for in the histological analyses. To measure relationships between long bone morphology, microstructure and *in vivo* loading accurately, the same animals should be accounted for in both the mechanical and the histological analyses. In the present study, the role that mechanical influences play during the ontogenetic development of long bone form and microstructural architecture was examined at the radius midshaft in three age groups of domestic goats (*Capra hircus*), specifically examining how regional patterns of cortical bone growth, porosity, remodelling and collagen fibre orientation relate to regional mechanical environments within the bone cortex.

This study tested the following hypotheses: (1) although bone growth in the goat radius does not result in the maintenance of similar strain magnitudes during ontogeny (Main & Biewener, 2004), the greatest rates of periosteal growth in the radius will occur where strains are greatest (Frost, 1983; Beaupré et al. 1990; Robling et al. 2001). Such a growth response will help to ensure safe strain magnitudes and the uniform strain patterns observed previously for this bone (Biewener & Taylor, 1986; Main & Biewener, 2004). (2) The greatest amounts of bone remodelling will coincide with the regions of highest strain, as these are where damage to the bone tissue is most likely to occur. Similarly, more remodelling is expected to be present in the radii of adult goats, as the bones of older animals are more likely to accumulate tissue damage. (3) As has generally been found for the horse radius (Boyde & Riggs, 1990; Riggs et al. 1993a; Mason et al. 1995), collagen fibre orientation will correlate with regional mechanical environments in the goat radius, with longitudinal and oblique/transverse fibres being most strongly correlated with regions of maximum tension and compression, respectively. (4) Additionally, the relatively unorganized, woven-fibred bone typical of young mammals (Francillon-Vieillot et al. 1990), and expected in the radii of juvenile goats, will show progressive regional differentiation in CFO through remodelling, as strain magnitudes increase during ontogeny (Main & Biewener, 2004).

Table 1 Sex, age, and mass for the goats included in the study

Group	Sex	Age (weeks)	Mass (kg)
Small	M	2.9	2.9
	M	3.7	3.3
	M	3.7	3.6
	F	13.4	4.8
	F	4.9	4.9
	F	5.7	6.0
Mean ± SD		5.5 ± 4.0	4.2 ± 1.2
Intermediate	M	13.4	6.8
	F	12.3	8.0
	M	10.9	11.8
Mean ± SD		12.2 ± 1.3	8.8 ± 2.6
Adult	M	39.0	15.6
	F	41.0	16.0
	F	48.9	17.4
	M	61.0	24.7
	F	124.3	33.0
Mean ± SD		62.8 ± 35.4	21.3 ± 7.5

Materials and methods

Animals

Domestic goats (*Capra hircus* L.) were obtained from a breeding population housed in large outdoor paddocks at Harvard University's Concord Field Station. Animals were either fed from their mothers or by available foliage, supplemented with hay and ruminant chow during the winter months. The 14 goats included in this study were grouped into three size classes ('small': ≤ 6 kg; 'intermediate': between 6 and 12 kg; and 'adult': > 15 kg), which also generally separated the goats by age (Table 1). Each goat was given a single intramuscular injection of calcein (30 mg kg^{-1}) prior to *in vivo* strain data collection and/or the animals being killed. Although there was some variation within each size/age group, the interval between the calcein injection and either surgery or the animals being killed was adjusted so that this interval was shorter in younger goats and longer in older goats, to reflect the presumably slower bone growth rates in the older animals (small: 9 ± 8 days, range 1–17 days; intermediate: 17 ± 2 days, range 15–18 days, adult: 19 ± 15 days, range 10–46 days; mean ± SD). One of the three intermediate goats (10.9 kg, Table 1) did not receive a calcein injection, so periosteal and endosteal bone growth rates could not be measured for this goat. However, the goat was included for bone strain and other histomorphometric measurements.

Bone strain data collection

In vivo bone strains for the two smaller groups, cross-sectional bone geometry and histomorphometric data were collected from the mid-shaft of each goat's left radius. The bone strain and cross-sectional geometry data have been presented previously (Main & Biewener, 2004) for six of the small goats and two of the intermediate goats included here, while cross-sectional geometry data have been presented for three of the adult goats included here.

The surgical and experimental procedures used in this study have been described previously (Biewener & Taylor, 1986; Main & Biewener, 2004). Briefly, strain gauges were attached under sterile surgical conditions to the left radius of each goat in the two smaller groups. Bone strains were not collected for the adult goats included in this study, but are based on data reported previously for the radii of three adult goats (Biewener & Taylor, 1986). For all three size groups, three-element rosette strain gauges were attached to the cranial and caudal bone surfaces at the radius's mid-shaft with quick-drying cyanoacrylate adhesive. In the two smaller groups an additional single-element strain gauge was attached to the medial surface of the radius. The goats were allowed 24–48 h to recover from surgery, over which time an injectable analgesic was given to mitigate potential effects of lameness. *In vivo* bone strains were then collected as the goats ran over a range of speeds and gaits either over ground or on a motorized treadmill. Lateral-view digital video, synchronized to the strain data, was simultaneously collected at 125 Hz to measure foot down and foot off times. Following strain data collection the goats were killed and their radii dissected for histomorphometric analysis. All surgical and experimental procedures were in accordance with and approved by Harvard University's Institutional Animal Care and Use Committee.

Following dissection from the soft tissues, the bones were allowed to dry at room temperature for at least 1 week. After measuring the alignment of the strain gauges relative to the long axis of the radius (longitudinal gauge: ±3° relative to the long axis) and their placement relative to the bone's midshaft, the radii were embedded in fibreglass resin. Two 100-μm thin sections were taken at the site of gauge placement (6 ± 5% of the bone's length from the midshaft, mean ± SD) using a diamond-bladed annular saw. All soft tissue and marrow were cleaned from the medullary

cavity. After affixing the sections to microscope slides, a magnified digital image of one entire cross-section for each goat was taken using a digital camera attached to a computer. The periosteal and endosteal surfaces of the bone image were traced in Photoshop, creating an outline of the cross-section from which the cross-sectional area and maximum and minimum second moments of area (I_{MAX} and I_{MIN}, respectively) were calculated using a custom macro for NIH Image 1.61.

Regional bone strain analyses

The strain analyses described here were based on data from trials in which the goats were galloping. Galloping typically induced the greatest strains in the radius, which are more likely to have an influential effect on possible relationships between bone form and mechanics than would the lower strains that occur at lower speed gaits (Rubin & Lanyon, 1982; Mosley et al. 1997; Robling et al. 2001; Burr et al. 2002). Because bending and axial compressive strains represent the majority of the strain within the radius at all ages (Main & Biewener, 2004), a custom Matlab routine was used to calculate mid-shaft cross-sectional planar longitudinal strain distributions at each point in time for the two smaller groups, using data from the three longitudinal gauge elements of each gauge (Biewener, 1992) for three to five strides (both stance and swing phases) for each trial. The calculated strain distributions were mapped on to the outlines of each mid-shaft cross-section. Owing to the computational demands of this analysis, the strain data were re-sampled from 2 kHz to 250 Hz. This down-sampling did not significantly affect the strain magnitudes or distributions.

Calculating the planar axial strain distributions for the radii of the adult goats used in this study was complicated by two factors. First, as noted above strain data were not collected from the adult goats whose radii were included here. However, using the peak maximum and minimum principal strain data collected previously for the cranial and caudal bone surfaces in adult goats and the angular orientation of these strains relative to the long axis of the radius (Biewener & Taylor, 1986), it was possible to back-calculate the raw axial strains for that single point in time. These axial strains were applied to the cranial and caudal surfaces of the radii for the adult goats used here. Second, strain data from three locations around the bone's cortex are required to calculate the normal cross-sectional strain distribution. The axial strains corresponding to the peak principal tension and compression for the cranial and caudal bone surfaces, respectively, were positioned to act half-way along the medio-lateral axis of the cross-section on each of the two bone surfaces, while a point of zero strain for each adult was determined by estimating the position of the neutral axis in the adult goat cross-sections. The position of the neutral axis for the adult goats was estimated by using the mean orientation of the neutral axis calculated for the small and intermediate goats over a series of strides. This resulted in a neutral axis for the adults, which was forced to pass through the centroid of the bone cross-section and was orientated 81° anticlockwise from I_{MIN} (Fig. 1A), running in a cranio-medial to caudo-lateral direction. This position for the neutral axis and the distribution of strains on the cranial and caudal bone surfaces at this single time point resulted in the cranial and lateral surfaces being loaded in tension and the caudal and medial surfaces being loaded in compression. Although this procedure assumes a neutral axis orientation and is limited to a single time point in the loading cycle, it provides a reasonable estimate at the cross-sectional strain distribution in the adults, which is fairly similar to those reported in the two smaller groups (Biewener & Taylor, 1986; Main & Biewener, 2004).

Once the cross-sectional strain distributions were calculated, each cross-sectional bone outline was divided into eight subsections, defined by the bone's I_{MAX} and I_{MIN} axes, with each quarter then bisected (Fig. 1A). Using the cross-sectional strain distributions the following strain or mechanical variables were determined for each of the eight subsections: maximum tension, minimum compression, maximum range (maximum tension + |minimum compression|), maximum radial and circumferential strain gradients and maximum longitudinal strain rates.

The maximum tension, minimum compression and maximum range for each subsection were calculated as follows. As the cross-sectional strain distribution changed iteratively from one time interval to the next over the series of strides examined for each trial (e.g. times X, Y and Z in Fig. 1A), the maximum tensile and minimum compressive strains, measured in quantities of microstrain ($\mu\varepsilon$, $\varepsilon \times 10^{-6}$), for each pixel were found and recorded (illustrated in Fig. 1A). The maximum values for all of the pixels throughout each bone subsection were then averaged, resulting in a mean value for peak tension, compression and strain range for each

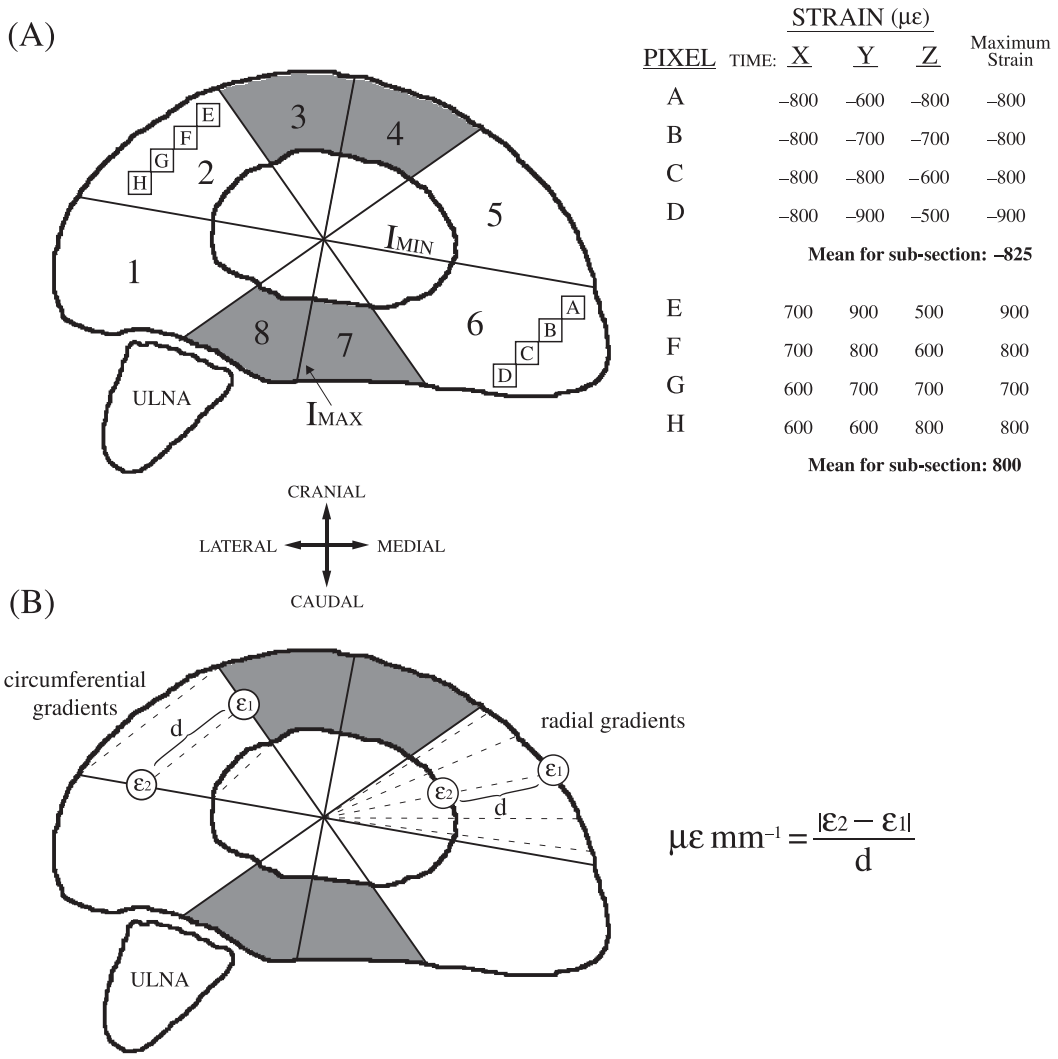

Fig. 1 (A) Illustration of the mid-shaft cross-section of the left radius from an intermediate goat divided into eight subsections using the axis about which the maximum second moment of area is distributed (I_{MAX}), the I_{MIN} axis, and two lines orientated at 45° relative to I_{MAX}. 'Pixels' A–D in subsection 6 and 'pixels' E–H in subsection 2 are shown to describe the method used to determine the mean peak strain magnitudes for each bone subsection. Hypothetical bone strains, measured in microstrain (με, strain $\times 10^{-6}$), for each of these 'pixels' is indicated at times X, Y and Z. The shaded regions represent the cranial (subsections 3 and 4) and caudal (subsections 7 and 8) regions of the bone. I_{MAX} and I_{MIN} are the axes about which the maximum and minimum second moments of area are distributed, respectively. The ulna is positioned caudo-lateral to the radius. (B) Illustration showing the method used to calculate the radial and circumferential strain gradients. To calculate the radial gradients, bone strains at two points along the periosteal and endosteal surfaces (ε1 and ε2) were sampled along the five guide lines for each subsection. To calculate the circumferential gradients, ε1 and ε2 were taken along the bounding lines of each subsection at the periosteal, endosteal and mid-cortical levels. For both gradient measurements, the absolute differences between ε1 and ε2 were divided by the distance between them (*d*) to determine the strain gradient (με mm^{-1}).

subsection. The mean peak strain values for each subsection were then averaged over the number of trials analysed for each goat, giving a mean value for each subsection of the bone for each goat.

The longitudinal strain rates during stance were found similarly by evaluating every pixel in each of the eight subsections. Each stance phase was divided into ten equal time periods. Within each time period, the strain rate for each pixel was determined similarly through a time-iterative process, dividing the difference in strain from one time point to the next at each pixel by the time elapsed (0.004 s for the 250-Hz sampling rate), resulting in a measurement of strain rate in units of strain per second (ε s^{-1}). The peak strain rate for each pixel during each of the ten time divisions was recorded. For each stance phase in each trial, a mean of

all the pixels in each subsection was determined for all of the ten time divisions. The peak strain rate for each time division was then averaged over the number of strides per trial and subsequently the number of trials analysed for each goat, resulting in one longitudinal strain rate value per bone subsection for each goat for each of the ten time divisions. The maximum longitudinal strain rate for each of the eight bone subsections for each goat was then determined as the maximum strain rate found for each subsection regardless of in which time division it occurred, resulting in a single maximum longitudinal strain rate value for each subsection for each goat.

To calculate the maximum radial and circumferential strain gradients, instead of sampling the entirety of each bone subsection, the gradients were determined by accounting for the differences in strains at defined points in each subsection. To calculate the peak radial gradients, five measurements were taken using guidelines plotted at 5, 13.75, 22.5, 31.25 and 40° relative to the bounding lines of each subsection (Fig. 1B). The normal strain values ($\varepsilon 1$ and $\varepsilon 2$ in Fig. 1B) and the positional coordinates of the two points on the endosteal and periosteal bone surfaces lying along these guidelines were recorded. At each point in time over a series of strides the radial strain gradient along each line was calculated as the difference in strain between the two points divided by their distance apart (*d* in Fig. 1B), resulting in a strain rate measured in microstrain per mm ($\mu\varepsilon\ mm^{-1}$; Gross et al. 1997; Judex et al. 1997). This was done iteratively through time with the peak radial gradient for each bone subsection during each trial taken as the absolute maximum average of the five lines during that trial. The mean length of the five guidelines was also taken to be the mean cortical thickness for each bone subsection.

The circumferential strain gradients were calculated similarly, except only three measurements were taken between each bone subsection's bounding lines at the periosteal, endosteal and mid-cortical levels (Fig. 1B). The peak average of the three measurements over time was taken as the peak circumferential gradient for each bone subsection.

Histomorphometric analyses

Two 100-μm thin-sections for each goat were visualized using an Olympus SZH10 microscope with a digital camera attachment connected directly to a computer (1 pixel = 0.00167 mm, 1280×1024-pixel resolution). IP Lab was used to capture images of each cross-section under plain, epifluorescent and circularly polarized light. At this level of magnification, a series of images were taken for each bone thin-section under each lighting condition and reassembled using PanaVue image software. The bounding lines outlining the positions of the eight subsections were overlaid on each composite image.

The plain light images were used to determine bone porosity and remodelling density. Bone porosity was measured as the density of vascular canals and resorption spaces in each subsection. The amount of remodelling that had occurred in each subsection was determined by measuring the density of 2° osteons (Haversian systems) and resorption spaces. Each density was measured using common stereological techniques (Martin et al. 1998). Using a custom Matlab routine, a rectangular grid was overlaid within each subsection of the composite cross-sectional image. Each grid was composed of lines spaced 0.17 mm apart. This constant line spacing varied the number of samples available per subsection, based upon differences in subsection area, but sampled each subsection equally at 36 samples per mm^2. The numbers of pores or 2° osteons that encountered gridline intersections were recorded and divided by the area of the grid, resulting in a measure of pores or 2° osteons per mm^2. These measurements were repeated three times for a single cross-section from each goat and the average measurement used to represent each subsection for that goat.

The periosteal and endosteal growth rates for each bone subsection were measured using the epifluorescent light images to visualize the calcein deposited in the bone. The distances between the periosteal and endosteal calcein labels and the periosteal and endosteal bone surfaces were divided by the number of days between which the label was given and either the time the periosteum was surgically removed or the goat was killed to yield a $\mu m\ day^{-1}$ measure of periosteal or endosteal accretional bone growth, respectively. Ten distance measurements were made perpendicular to either the endosteal or the periosteal bone surfaces within each subsection and the mean of the ten measurements taken. This was repeated three times for a single cross-section from each goat and the average measurement used to represent each subsection for that goat.

Circularly polarized light (CPL) microscopy was used to measure the relative collagen fibre orientations in

each bone subsection (Boyde & Riggs, 1990; Bromage et al. 2003). Similar to previous methods, each composite CPL was converted to a greyscale image in Photoshop. Each bone subsection was then overlaid with a grid of intersecting lines comprising 121 fixed intersection points and, thus, a variable sampling frequency (samples mm^{-2}), dependent upon the area sampled. Because this measurement was used simply to characterize each subsection, not to obtain a specific density measure, it was considered more important to maintain a consistent number of samples than sampling frequency. Each intersection was sampled unless it coincided with a vascular canal or resorption space. A greyscale value was recorded for each sampled pixel. Pixel greyscale values (% white) between 0 and 33% appeared dark and represented fibres orientated primarily longitudinally in the bone's cortex or parallel to the long axis of the bone. Values between 67 and 100% appeared white, which represented fibres orientated transversely in the section or perpendicular to the long axis of the bone. Finally, pixels with greyscale values between 34 and 66% represented obliquely orientated fibres.

Because variation in section thickness can affect CPL greyscale values, two separate 100-μm thin-sections were each sampled once to give a mean for each subsection for each goat, accounting for whatever minor variation in thickness may have existed between serial thin-sections or regional differences in thickness within a given bone cross-section. Additionally, CPL greyscale values are affected by mineral content within the bone, with less well-mineralized bone appearing brighter than more highly mineralized bone of similar thickness (Boyde & Riggs, 1990). The mineral content of the radius mid-shaft was significantly greater in the adult goats (Main & Biewener, 2004), so comparison of the fibre orientations across age cannot meaningfully be made. However, different bone subsections within a size group can be compared, assuming relatively similar section thickness between the bone subsections for a given goat.

Statistics

Statistical tests were conducted to examine the differences in mechanical strain environment and histomorphometry between both the different age groups and the eight bone subsections. Where possible, separate one-way ANOVAs (SPSS v13.0) were used to test for differences between the bone subsections or age groups. When significant differences were found Bonferroni *post-hoc* tests determined what specific factors caused these differences. If the data used in any test were found to have inhomogeneous variance (SPSS; Dytham, 2003), the non-parametric Kruskall–Wallis test was used. When significant differences were found using this test, the Mann–Whitney *U*-test determined which age groups or subsections were responsible for the differences. Differences were considered significant at $P < 0.05$.

Because a major focus of this work is to determine if the histomorphometric and mechanical strain characteristics are significantly related, partial correlation tests of the measured histomorphometric and strain characteristics were also conducted, controlling for the effects of age/size group. As there were 14 variables examined, resulting in 91 separate correlation tests, the probability of finding a significant result at the $P < 0.05$ level by chance was fairly high. Thus, the Bonferroni method for reducing the critical *P*-value ($P < 0.05/91 = 0.00055$; Dytham, 2003) was used in these analyses to determine significant correlations between the different variables examined.

Results

Periosteal and endosteal bone growth

Periosteal growth rates decreased with age and were not uniform around the bone's cortex in any of the three age groups. Periosteal growth rates were generally greater in the small vs. the intermediate goats (Fig. 2A, Table 2), although this difference was not significant ($P = 0.285$). However, both smaller groups had significantly greater periosteal growth rates than the adult goats ($P < 0.005$ for both groups). Although the growth rates changed with age, similar non-uniform regional growth patterns were maintained during ontogeny, with greater periosteal accretional growth occurring on the medial and lateral bone surfaces than on the cranial and caudal surfaces (Fig. 2A, Table 2). Periosteal growth rates in sections 1 and 6, on the lateral and medial bone surfaces, respectively, were significantly greater than the growth rates in sections 3, 7 and 8 on the cranial and caudal surfaces. Sections 1 and 5 also showed significantly higher growth rates than sections 4 and 7, respectively.

Such clear differences in regional and even age-related patterns were not evident for the endosteal growth rates. There was no difference in endosteal growth rates

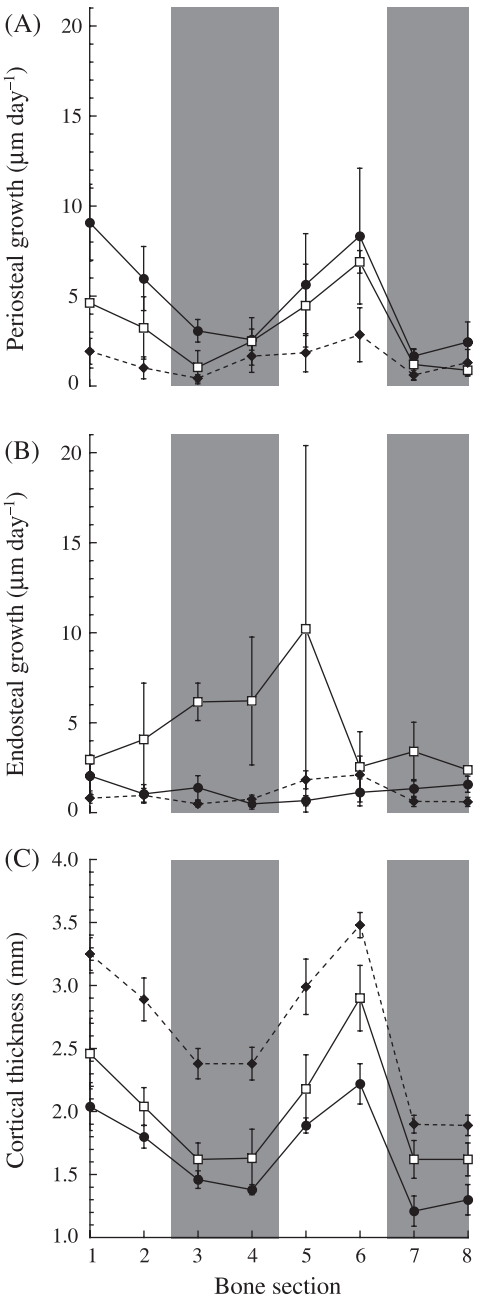

Fig. 2 (A) Periosteal growth rates, (B) endosteal growth rates and (C) cortical thickness vs. bone section for the three age groups. Numbers 1–8 on the *x*-axis refer to the numbered bone subsections in Fig. 1. Each point represents the mean ± SE. Sample sizes for each group are given in Table 2. The following symbols represent each group: small (●), intermediate (□) and adult (◆). The shaded bars indicate the cranial (subsections 3 and 4) and caudal (subsections 7 and 8) regions of the bone. As in Table 2, because $N = 2$ for the intermediate group, the error bars simply represent the difference between each of the two data points and the mean.

between the small and adult goats (Fig. 2B, Table 2, $P = 0.88$), but the intermediate group showed significantly greater endosteal growth than either of the other two groups ($P < 0.001$). It should be noted, however, that cortical growth rates were only obtained for two of the three intermediate goats and in some subsections the two goats showed very different endosteal growth rates from one another, explaining the large standard errors for the intermediate group in certain subsections. Unlike at the periosteum, there was no consistent significant difference in growth rates between the different bone subsections ($P = 0.952$).

Differential regional cortical growth rates, primarily on the periosteum, resulted in overall bone growth patterns at the radius mid-shaft that produced greater expansion of the bone in the medio-lateral direction relative to the cranio-caudal direction during ontogeny. Cortical thickness in all subsections increased progressively and significantly from one age group to the next (Fig. 2C, Table 2, $P < 0.02$ between all groups). However, these increases were generally greater on the medial and lateral surfaces of the radius than on the cranial and caudal surfaces, as medio-lateral subsections 1, 2, 5 and 6 were significantly thicker than caudal subsections 7 and 8, while subsections 1 and 6 were also significantly thicker than cranial sections 3 and 4 (Fig. 2C).

The regional differences in cortical thickness and asymmetric cortical expansion were established early in growth, as the greatest disparity in growth rates between the different subsections occurred among the small goats, with the thickest subsections having the highest periosteal growth rates (Fig. 3A). However, the slope of the line describing this trend in the small goats (16.3 ± 4.2, slope ± 95% CI) was not significantly different from that for the intermediate group (12.4 ± 3.3). Both smaller groups showed greater non-uniformity in regional growth than the adults (Fig. 3A, slope: 3.4 ± 3.1). Although periosteal growth rates decreased with age, adults still showed significant differences in regional growth, continuing to elaborate upon the asymmetries in regional cortical thickness established in the younger animals. A schematic representation of these cortical growth patterns is illustrated in Fig. 3(B).

Porosity and remodelling

There were significant differences in porosity and remodelling densities between the different age groups, but differences between the different bone subsections

Table 2 Histomorphometric measurements for each group and bone subsection

			Bone subsection							
	Units	Group	1	2	3	4	5	6	7	8
Periosteal growth	μm day^{-1}	Small	9.1 ± 2.1	6.0 ± 1.8	3.1 ± 0.6	2.6 ± 0.6	5.6 ± 2.8	8.3 ± 3.8	1.7 ± 0.4	2.4 ± 1.1
		Intermediate*	4.6 ± 0.1	3.2 ± 1.7	1.1 ± 0.9	2.5 ± 1.3	4.5 ± 2.3	6.9 ± 0.6	1.2 ± 0.9	0.9 ± 0.3
		Adult	1.9 ± 0.7	1.0 ± 0.6	0.4 ± 0.2	1.7 ± 0.9	1.9 ± 1.1	2.9 ± 1.5	0.6 ± 0.3	1.3 ± 0.7
Endosteal growth	μm day^{-1}	Small	2.1 ± 0.9	1.1 ± 0.5	1.4 ± 0.7	0.5 ± 0.3	0.7 ± 0.3	1.1 ± 0.8	1.3 ± 0.5	1.5 ± 0.5
		Intermediate*	3.0 ± 0.3	4.1 ± 3.1	6.2 ± 1.0	6.2 ± 3.6	10.2 ± 10.2	2.6 ± 2.0	3.4 ± 1.6	2.4 ± 0.0
		Adult	0.8 ± 0.3	1.0 ± 0.4	0.5 ± 0.2	0.8 ± 0.2	1.8 ± 0.5	2.1 ± 1.0	0.6 ± 0.3	0.6 ± 0.3
Cortical thickness	mm	Small	2.0 ± 0.2	1.8 ± 0.1	1.5 ± 0.1	1.4 ± 0.0	1.9 ± 0.1	2.2 ± 0.2	1.2 ± 0.1	1.3 ± 0.1
		Intermediate	2.5 ± 0.3	2.0 ± 0.2	1.6 ± 0.1	1.6 ± 0.2	2.2 ± 0.3	2.9 ± 0.3	1.6 ± 0.2	1.6 ± 0.1
		Adult	3.3 ± 0.1	2.9 ± 0.2	2.4 ± 0.1	2.4 ± 0.1	3.0 ± 0.2	3.5 ± 0.1	1.9 ± 0.1	1.9 ± 0.1
Porosity	pores mm^{-2}	Small	4.6 ± 0.7	4.2 ± 0.5	4.4 ± 0.7	5.0 ± 0.9	5.4 ± 0.8	4.8 ± 0.6	4.5 ± 1.3	6.2 ± 0.8
		Intermediate	3.5 ± 0.1	3.5 ± 0.7	4.3 ± 0.7	3.5 ± 0.5	4.9 ± 0.3	4.2 ± 0.2	3.2 ± 1.2	4.0 ± 0.3
		Adult	2.8 ± 0.6	2.5 ± 0.6	2.5 ± 0.9	2.9 ± 1.0	3.1 ± 0.7	2.9 ± 0.7	2.9 ± 0.6	3.7 ± 0.6
Remodelling	2° osteons mm^{-2}	Small	1.4 ± 1.1	0.2 ± 0.2	0.3 ± 0.2	0.4 ± 0.3	0.3 ± 0.2	0.8 ± 0.5	1.6 ± 0.6	1.3 ± 0.6
		Intermediate	2.3 ± 0.6	3.1 ± 1.4	3.5 ± 1.7	2.1 ± 1.5	3.0 ± 1.5	3.6 ± 0.9	7.6 ± 0.4	6.4 ± 1.2
		Adult	12.0 ± 2.3	14.0 ± 2.4	14.9 ± 1.7	12.2 ± 1.5	9.4 ± 2.8	14.6 ± 2.7	15.5 ± 1.7	16.5 ± 2.4
% Longitudinal fibres	%	Small	77 ± 4	80 ± 3	77 ± 2	77 ± 3	83 ± 2	79 ± 3	60 ± 3	56 ± 4
		Intermediate	75 ± 5	72 ± 4	75 ± 4	78 ± 5	81 ± 5	75 ± 5	57 ± 6	55 ± 5
		Adult	63 ± 3	59 ± 3	63 ± 4	63 ± 4	70 ± 2	68 ± 2	48 ± 3	46 ± 4
% Oblique fibres	%	Small	14 ± 2	13 ± 2	14 ± 1	16 ± 3	11 ± 2	14 ± 2	23 ± 2	24 ± 2
		Intermediate	16 ± 3	17 ± 3	13 ± 3	12 ± 3	9 ± 1	14 ± 3	20 ± 2	20 ± 1
		Adult	17 ± 2	18 ± 1	17 ± 1	16 ± 1	15 ± 1	17 ± 1	20 ± 1	21 ± 1
% Transverse fibres	%	Small	9 ± 2	7 ± 2	8 ± 1	7 ± 1	5 ± 1	7 ± 2	18 ± 2	21 ± 2
		Intermediate	10 ± 2	11 ± 1	12 ± 2	10 ± 3	10 ± 4	10 ± 2	23 ± 4	26 ± 4
		Adult	20 ± 3	23 ± 3	20 ± 3	20 ± 4	15 ± 2	15 ± 2	32 ± 4	33 ± 4

Values shown are mean ± SE.
Small: n = 6; intermediate: n = 3; adult: n = 5.
*n = 2, so ± SE simply describes the difference between each of the two data points and the mean.
Bone subsection numbers 1–8 correspond to the subsection numbers in Fig. 1.

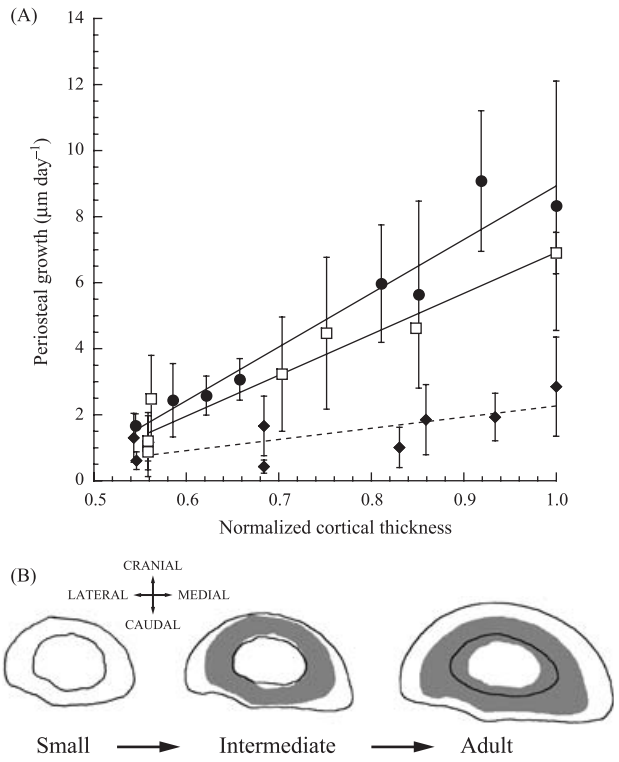

Fig. 3 (A) Periosteal growth rate vs. cortical thickness normalized by the thickest cortical region. Each point represents the mean ± SE. The following symbols represent each group: small (●), intermediate (□) and adult (◆). Each line is the least-squares regression fit to the data for each age group. Small: $y = -7.3 + 16.3x$ (± 4.2, ± 95% CI, $R^2 = 0.94$), intermediate: $y = -5.5 + 12.4x$ (± 3.3, $R^2 = 0.93$), adult: $y = -1.1 + 3.4x$ (± 3.1, $R^2 = 0.55$). Sample sizes are given in Table 2. As in Table 2, because $n = 2$ for the intermediate group, the error bars simply represent the difference between each of the two data points and the mean. (B) Sample radius cross-sections for each age group illustrating the changes in cross-sectional geometry with growth. The grey shadows in the intermediate and adult bones are the cross-sections from the small and intermediate groups, respectively, to emphasize the changes with age/size. Each bone cross-section is a representative of each group, but the cortical thicknesses and changes in endosteal and periosteal diameters from one group to the next do not directly correspond to the means presented in Fig. 2 or Table 2. The ulna has been omitted for clarity.

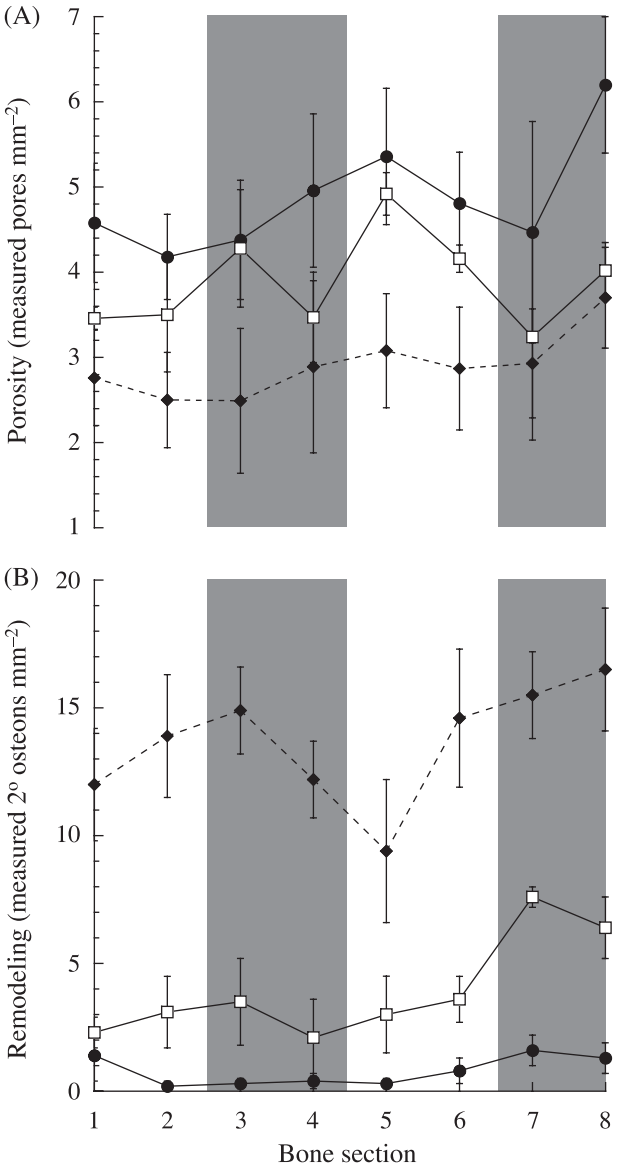

Fig. 4 (A) Measured porosity and (B) remodelling densities vs. bone section. Numbers 1–8 on the *x*-axis refer to the numbered bone subsections in Fig. 1. The following symbols represent each group: small (●), intermediate (□) and adult (◆). Each point represents the mean ± SE. Sample sizes are given in Table 2. The shaded bars indicate the cranial (subsections 3 and 4) and caudal (subsections 7 and 8) regions of the bone.

were less obvious. Porosity decreased across the three groups as the small goats had significantly more porous bones than the intermediate (Fig. 4A, Table 2, $P = 0.043$) and adult groups ($P < 0.001$). Similarly, the intermediate aged goats had more porous bones than the adults ($P = 0.004$). Due to high inter-individual differences within each age group, no significant differences in porosity were found between the different bone subsections.

Remodelling within the radius increased significantly during ontogeny (Fig. 4B, Table 2, $P < 0.001$ between all groups). Similar to patterns of porosity, however, no significant trends in the distribution of remodelling between the different subsections were observed. However, in the intermediate age group subsection 7 generally showed greater remodelling than other

subsections of the radius. In adults, although relatively less remodelling generally occurred in subsection 5, it was not significantly different from the other subsections.

Collagen fibre orientation

Although the orientation of collagen fibres within the goat radius cannot be quantitatively compared between the different age groups because of age-related differences in mineralization, within each group the radii did show significant regional differences between the bone subsections. Although showing no significant differences between each other, subsections 1–6 had a significantly higher percentage of longitudinal fibres in all three age groups and a lower percentage of transverse and oblique (not shown) fibres than subsections 7 and 8, which correspond to the caudal region of the bone (Fig. 5, Table 2). Although not directly comparable, the more highly mineralized radii of the adult group (Main & Biewener, 2004) appeared brighter under CPL, resulting in the seemingly higher percentage of transverse collagen than in the less well-mineralized bones of the two smaller groups.

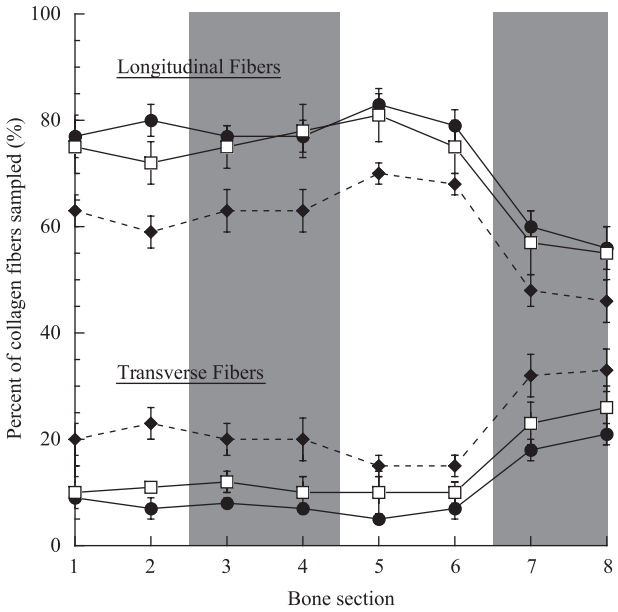

Fig. 5 Collagen fibre orientation vs. bone section. Collagen fibre orientations are presented as the percentage of the total collagen fibres sampled in each bone section. Numbers 1–8 on the *x*-axis refer to the numbered bone subsections in Fig. 1. The following symbols represent each group: small (●), intermediate (□) and adult (◆). Each point represents the mean ± SE. Sample sizes are given in Table 2. The three lines at the top of the figure correspond to measurements of the longitudinal fibres while the three lines at the bottom of the figure correspond to the percentage of transverse fibres measured. Data for the oblique fibres measured were omitted for clarity. The shaded bars indicate the cranial (subsections 3 and 4) and caudal (subsections 7 and 8) regions of the bone.

Maximum tension, compression, and strain range

Generally, peak tensile and compressive strains and the maximum strain ranges increased in each subsection during ontogenetic growth. Each progressively larger, older group of animals showed significant increases in tensile and compressive strains (Table 3, tension: $P < 0.05$, compression: $P < 0.005$ for all between-group comparisons). As a result, the peak strain ranges experienced by each bone subsection also increased with size between the small and intermediate groups (Table 3, $P < 0.001$). Because cross-sectional strain distributions were only determined at a single time for the adult group, strain ranges and values of peak tensile and compressive strains for all eight subsections could not be determined for the adults.

The magnitudes of the peak tensile and compressive strains also differed between the different bone subsections (Table 3). Tensile strains were significantly greater in subsections 1–3 (cranio-lateral) than in sections 4–7. Compressive strains in subsections 1–4 were significantly lower (less compression) than in sections 5–7. If the adult goats, with their much greater peak strains and more limited regional peak strain data (Table 3), are removed from the statistical analysis, significant differences in peak strains between the different subsections in the two smaller groups are still generally maintained, although more regionally restricted. Considering only the two smaller groups, peak tensile strains in subsections 1–3 were significantly greater than subsection 5 (but not 4, 6 or 7). Correspondingly, only sections 2 and 3 showed significantly lower compressive strains than sections 5–7, while subsections 1 and 4 showed significantly lower compression than only section 6.

Finally, the distribution of maximum strain ranges across the different subsections in the small and intermediate groups showed no significant regional variation (Table 3, $P = 0.542$).

Strain gradients and longitudinal strain rates

Just as peak strain magnitudes increased with size and age, so did the measured strain gradients and longitudinal

Table 3 Maximum strains, strain gradients and longitudinal strain rates for each group and bone subsection

			Bone subsection							
	Units	Group	1	2	3	4	5	6	7	8
Tensile strain	με	Small	385 ± 106	443 ± 133	330 ± 74	227 ± 39	162 ± 18	221 ± 37	206 ± 52	235 ± 47
		Intermediate	530 ± 135	479 ± 212	449 ± 176	329 ± 104	181 ± 23	268 ± 65	347 ± 77	405 ± 76
		Adult	3261 ± 221	3296 ± 175	1235 ± 67	*	*	*	*	559 ± 88
Compressive strain	με	Small	−328 ± 60	−291 ± 42	−351 ± 66	−465 ± 54	−658 ± 93	−801 ± 130	−596 ± 116	−460 ± 108
		Intermediate	−1040 ± 440	−713 ± 245	−566 ± 179	−615 ± 155	−811 ± 226	−1171 ± 141	−1213 ± 167	−1210 ± 319
		Adult	*	*	*	−656 ± 55	−2819 ± 128	−3500 ± 113	−1152 ± 69	*
Strain range	με	Small	712 ± 93	733 ± 140	681 ± 122	691 ± 84	820 ± 103	1012 ± 141	803 ± 143	695 ± 113
		Intermediate	1570 ± 316	1192 ± 78	1015 ± 244	944 ± 257	992 ± 241	1439 ± 205	1560 ± 186	1614 ± 303
		Adult	*	*	*	*	*	*	*	*
Radial gradient	με mm^{-1}	Small	171 ± 36	172 ± 34	139 ± 20	132 ± 28	172 ± 36	173 ± 34	139 ± 20	133 ± 28
		Intermediate	200 ± 33	267 ± 26	275 ± 24	178 ± 55	200 ± 33	266 ± 26	276 ± 25	178 ± 55
		Adult	619 ± 59	691 ± 58	357 ± 24	185 ± 27	619 ± 59	689 ± 59	360 ± 23	184 ± 28
Circumferential gradient	με mm^{-1}	Small	185 ± 36	148 ± 21	141 ± 36	164 ± 35	187 ± 35	146 ± 22	143 ± 36	163 ± 34
		Intermediate	238 ± 43	231 ± 41	193 ± 27	187 ± 48	237 ± 55	211 ± 55	200 ± 22	188 ± 35
		Adult	614 ± 58	450 ± 47	709 ± 64	729 ± 62	610 ± 46	486 ± 60	701 ± 64	726 ± 64
Longitudinal strain rate	ε s^{-1}	Small	0.040 ± 0.013	0.025 ± 0.011	0.009 ± 0.004	0.010 ± 0.002	0.017 ± 0.005	0.012 ± 0.004	0.021 ± 0.005	0.032 ± 0.009
		Intermediate	0.102 ± 0.025	0.077 ± 0.021	0.031 ± 0.013	0.012 ± 0.003	0.028 ± 0.001	0.022 ± 0.003	0.039 ± 0.006	0.069 ± 0.015
		Adult	*	*	*	*	*	*	*	*

Values shown are mean ± SE.
Small: $n = 6$; intermediate: $n = 3$; adult: $n = 5$.
*No data for the adult goats as strain distributions could only be reconstructed for a single time point.
Bone subsection numbers 1–8 correspond to the subsection numbers in Fig. 1.

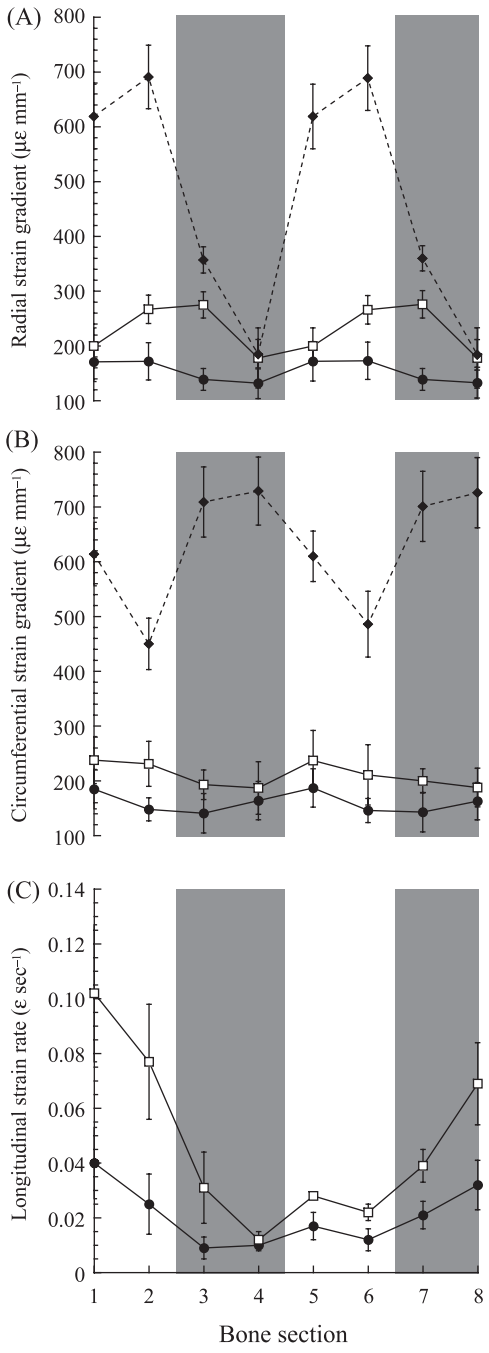

Fig. 6 (A) Radial strain gradients, (B) circumferential strain gradients and (C) longitudinal strain rates vs. bone section. Numbers 1–8 on the *x*-axis refer to the numbered bone subsections in Fig. 1. The following symbols represent each group: small (●), intermediate (□) and adult (◆). Each point represents the mean ± SE. Sample sizes are given in Table 3. Longitudinal strain rates could not be determined for the adult group. The shaded bars indicate the cranial (subsections 3 and 4) and caudal (subsections 7 and 8) regions of the bone.

strain rates. The circumferential and radial strain gradients increased progressively from one size group to the next (Fig. 6, Table 3, $P < 0.004$ and $P < 0.001$ between all groups, respectively). The longitudinal strain rates were also significantly greater in the intermediate than the small goats (Fig. 6C, $P < 0.001$).

Although differences in magnitude for the longitudinal strain rates and strain gradients existed between the three age groups, the regional patterns throughout the bones tended to be fairly consistent during ontogeny. The radial strain gradients showed similar regional patterns across the three groups, with sections 4 and 8 experiencing significantly lower radial strain gradients than the other subsections (Fig. 6A, $P < 0.05$). By contrast, the circumferential gradients showed no consistent differences between the different subsections, although the absence of any significant regional pattern was consistent across the three age groups (Fig. 6B). In the adult goat radii, the medial and lateral cortices (subsections 1, 2, 5 and 6) experienced greater radial and lower circumferential strain gradients. This is consistent with the fixed cross-sectional strain distributions for the adult goats about a neutral axis of bending orientated near the anatomical cranial–caudal axis, whereas varying the position of the neutral axis through time (as in the two smaller groups) would result in more uniform regional strain gradients.

Although the longitudinal strain rates could only be calculated for the two smaller groups, they both showed significant regional patterns (Fig. 6C). Subsection 4 generally experienced the lowest longitudinal strain rates (~0.01 $\varepsilon\ s^{-1}$), which were significantly lower than in subsections 1, 2, 7 and 8, where the strain rates ranged between 0.02 and 0.04 $\varepsilon\ s^{-1}$ in the small group and 0.04 and 0.10 $\varepsilon\ s^{-1}$ in the intermediate group. Consequently, there was about a two-fold increase in longitudinal strain rate with age. Additionally, the longitudinal strain rates in both subsections 1 and 8 were significantly greater than the strain rates in sections 3 and 6.

Correlations between the histological and mechanical variables

Many of the histological and mechanical variables examined correlated with cortical subsection thickness. Not surprisingly, periosteal growth rate correlated significantly with cortical thickness (Table 4, partial correlation coefficient: 0.374, $P = 0.0001$), whereas endosteal

growth rate did not ($P = 0.836$), indicating that regional cortical thickness was dependent upon periosteal but not endosteal apposition. Although greater tensile and compressive strains and greater radial gradients were correlated with the thicker cortical subsections as well (0.405, −0.483, 0.496, respectively, $P < 0.0002$ for all), periosteal growth rates did not correlate directly with these or any of the other measured mechanical strain variables (Table 4).

Some aspects of collagen fibre orientation also correlated with subsection cortical thickness. An increased percentage of longitudinal collagen fibres and thus a decrease in transverse collagen occurred in the thicker regions of the bones' cortices (0.340 and −0.332, respectively, $P < 0.0005$ for both). This correlation occurred regardless of the strain environments in these thicker subsections, as collagen fibre orientation was not directly correlated with the mechanical strain environment in any way, except for the percentage of transverse collagen being negatively correlated with radial gradients (–0.374, $P = 0.0001$).

The density of pores and remodelling within the bones' cortices did not show significant correlations with any of the mechanical variables measured. However, the negative correlation between remodelling and longitudinal strain rate was nearly significant (Table 4, −0.393, $P = 0.0007$). Both remodelling and porosity were also independent of cortical thickness, although remodelling was positively correlated with an increased percentage of transverse collagen fibres and a decreased percentage of longitudinal fibres (0.447 and −0.450, respectively, $P < 0.0001$ for both).

Discussion

Ontogenetic bone growth in relation to mechanical environment

In this study, natural physiological strain environments based on measurements from earlier studies (Biewener & Taylor, 1986; Main & Biewener, 2004) were determined for the goat radius during ontogeny and related to the cortical and endosteal growth rates in the same bones. This approach allows for the examination of the modelling and remodelling of bone shape in relation to ontogenetic patterns of functional strain under natural conditions. Most studies examining relationships between mechanical loading and cortical growth have often used invasive or exogenous loading models in either growing or adult animals. Nevertheless, these studies have been valuable in establishing that rates of appositional bone growth can correlate with one or more of the following: strain magnitude, strain frequency, strain rate and circumferential strain gradients within the bone cortex (Gross et al. 1997; Mosley et al. 1997; Mosley & Lanyon, 1998; Robling et al. 2001).

Natural, physiological *in vivo* bone strains in vertebrate long bones have previously only been related to quantitative measures of regional cortical growth in studies examining growth and adaptation to exercise in the tarsometatarsus (TMT) of growing and adult chickens (Judex et al. 1997; Judex & Zernicke, 2000). Periosteal and endosteal bone apposition rates in the TMT of growing chickens were not correlated with the measured strain environments (Judex & Zernicke, 2000). However, in adult chickens, periosteal growth was strongly correlated with peak circumferential strain gradients, but not associated with peak strain magnitudes or longitudinal strain rates (Judex et al. 1997). Similar to the TMT of growing chickens, but in contrast to the expected results, cortical growth in the goat radius was not significantly correlated with strain magnitudes, strain rates or strain gradients. The strain gradients and peak strain magnitudes in the regions loaded primarily under tension (subsections 1–3) or compression (subsections 5–7) generally did not differ significantly within each type of loading. Because of the differential periosteal growth in these various subsections, maintenance of the mechanical variables at similar levels resulted in an apparent lack of correlation between mechanical environment and regional growth rates.

Although strong negative ontogenetic allometry in the cross-sectional area and second moments of area (Main & Biewener, 2004) allowed for an ontogenetic increase in the magnitudes of the measured peak strains, strain gradients and strain rates, they generally increased in a regionally uniform fashion from one age group to the next (Fig. 6). This suggests that although cortical growth did not correlate directly with the measured strain characteristics, the regional patterns of bone modelling, and resulting cross-sectional shape asymmetry, may have helped to maintain the distribution of these characteristics during ontogeny. The goat radius showed clear growth asymmetries that were greatest in the younger goats but maintained in the older animals as well. This growth asymmetry produced much thicker cortices in the medio-lateral regions, which resulted in greater second moments of area and

Table 4 Partial correlation coefficients, *P*-values and sample sizes for the mechanical and histomorphological variables examined

	Cortical thickness	Periosteal growth	Endosteal growth	Porosity	Remodeling	% Longitudinal fibers	% Oblique fibers	% Transverse fibers	Tensile strain	Compressive strain	Strain range	Radial gradient	Circumferential gradient	Longitudinal strain rate
Cortical thickness														
Periosteal growth	**0.374** **0.0001** **101**													
Endosteal growth	−0.021 0.8361 101	−0.080 0.4242 101												
Porosity	−0.137 0.1504 109	−0.086 0.3893 101	−0.042 0.6757 101											
Remodeling	0.002 0.9822 109	−0.129 0.1945 101	−0.299 0.0021 101	−0.318 0.0007 109										
% Longitudinal fibers	**0.340** **0.0003** **109**	0.138 0.1661 101	0.232 0.0183 101	−0.081 0.3958 109	**−0.450** **< 0.0001** **109**									
% Oblique fibers	−0.278 0.0032 109	−0.078 0.4367 101	−0.222 0.0241 101	0.095 0.3212 109	**0.331** **0.0004** **109**	**−0.852** **< 0.0001** **109**								
% Transverse fibers	**−0.332** **0.0004** **109**	−0.153 0.1232 101	−0.197 0.0464 101	0.066 0.4934 109	**0.447** **< 0.0001** **109**	**−0.948** **< 0.0001** **109**	**0.644** **< 0.0001** **109**							
Tensile strain	**0.405** **0.0001** **89**	0.016 0.8850 81	−0.127 0.2535 81	−0.078 0.4600 89	0.025 0.8147 89	0.111 0.2965 89	−0.041 0.7032 89	−0.131 0.2156 89						
Compressive strain	**−0.483** **< 0.0001** **89**	−0.201 0.0692 81	−0.122 0.2706 81	−0.057 0.5943 89	0.048 0.6549 89	−0.284 0.0064 89	0.100 0.3441 89	0.341 0.0010 89	**0.983** **< 0.0001** **69**					
Strain range	0.088 0.4651 69	0.210 0.0978 61	**0.430** **0.0004** **61**	−0.054 0.6530 69	−0.230 0.0533 69	0.304 0.0100 69	−0.209 0.0803 69	−0.264 0.0263 69	0.012 0.9213 69	**−0.814** **< 0.0001** **69**				
Radial gradient	**0.496** **< 0.0001** **109**	0.140 0.1592 101	−0.011 0.9101 101	−0.128 0.1834 109	−0.155 0.1055 109	0.315 0.0008 109	−0.157 0.1001 109	**−0.374** **0.0001** **109**	**0.840** **< 0.0001** **89**	**−0.748** **< 0.0001** **89**	0.172 0.1523 69			
Circumferential gradient	−0.155 0.1047 109	−0.020 0.8422 101	−0.208 0.0347 101	−0.020 0.8335 109	0.115 0.2277 109	0.018 0.8549 109	0.004 0.9702 109	−0.036 0.7088 109	0.084 0.4296 89	0.181 0.0855 89	−0.394 0.0007 69	0.043 0.6510 109		
Longitudinal strain rate	−0.076 0.5303 69	0.162 0.2056 61	0.096 0.4565 61	0.147 0.2213 69	−0.393 0.0007 69	0.168 0.1606 69	−0.069 0.5651 69	−0.164 0.1714 69	−0.190 0.1134 69	−0.313 0.0079 69	0.393 0.0007 69	−0.106 0.3792 69	−0.322 0.0062 69	

Bold values represent significant correlations at the corrected $P < 0.00055$ value.

thus greater resistance to bending forces in the medio-lateral direction. Previously, such shape asymmetries have been argued to enhance load predictability in vertebrate long bones (Lanyon, 1987; Bertram & Biewener, 1988), reducing the risk of injury due to unexpected catastrophic loads. Although goats are born with asymmetrical second moments of area (I_{MAX}/I_{MIN} = 1.95 in 1-day-old goats), the active elaboration of this asymmetry following subsequent loading early in growth (I_{MAX}/I_{MIN} = 2.40 by about 3 weeks and 3.09 by 16 weeks) indicates the likely importance of this shape asymmetry as a fundamental feature of this bone's structural form in relation to its load-bearing function.

The load predictability argument has previously been invoked to suggest a more or less static bending orientation within the long bones during the stance phase of a locomotor stride. Recent *in vivo* bone strain studies, however, have shown that bending direction can vary during loading in subcircular bones (Biewener & Dial, 1995; Blob & Biewener, 1999; Lieberman et al. 2004; also see Pearson & Lieberman, 2004), but the variation in bending direction observed here for such an eccentrically shaped bone might be considered unexpected given previous theory (Bertram & Biewener, 1988). Even though the plane of bending within the radius typically rotates through nearly 180° during stance in the small and intermediate goats, regional patterns of strain were maintained more or less consistently through growth to maturity during steady, treadmill locomotion. At each stage of growth examined, the radii showed similar regional patterns for the measured mechanical variables, and a consistent correlation indicating that greater strain magnitudes occurred in the thicker cortices. The fact that the greatest strains occurred where the cortex was thickest reinforces the importance of asymmetrical periosteal growth in the medio-lateral cortices for effective load-bearing function.

The 'predictability' or relative consistency of regional strain patterns observed here during ontogeny may, in part, reflect the need to use the strain distributions observed in the two smaller groups to test correlations with bone modelling and remodelling patterns observed in the adult radii. Because only limited midshaft strain data exist for adult goats (Biewener & Taylor, 1986), the rotation of the neutral axis could not be traced through stance. However, because the relative limb loads and general kinematics do not change during growth (Main & Biewener, 2004), it is likely that the neutral axis undergoes rotation in the adult goats as well. At a minimum, there is no evidence to the contrary. Thus, natural selection appears to have favoured a growth strategy in the goat radius leading toward (if not a uniform bending orientation during weight support) relatively consistent time-varying regional strain patterns during ontogeny.

Porosity and remodelling in relation to regional mechanical environment

As with periosteal growth, porosity and remodelling have typically not been examined in association with specific regional mechanical environments during natural *in vivo* conditions. In the absence of any exogenous or experimental loads, regional differences in porosity have been found in some vertebrate long bones (turkey ulna, human femur; Skedros et al. 2003; Thomas et al. 2005) and the mule deer calcaneus (Skedros et al. 1994). In the human femur these regional patterns became more pronounced with age (Thomas et al. 2005). However, these studies did not directly measure regional mechanical environments within the bones examined, and the areas of greater porosity were hypothesized to be variably linked to remodelling initiated by mechanical microdamage (high strain; Skedros et al. 2003) or to disuse osteoporosis (low strain; Thomas et al. 2005). Additionally, in the femur, tibia and metatarsus of the sheep hind limb, remodelling initiated by increased levels of exercise generally occurred in specific anatomical regions (Lieberman et al. 2003), but was not, however, associated with a common type of strain environment among the different bones.

In contrast to the hypothesized results, porosity and remodelling in the goat radius did not correlate with any of the mechanical variables analysed here. Consistent with these results, no strong regional differences in porosity were observed in the horse radius mid-shaft either, which could also not be explained by regional strain environments (Mason et al. 1995). However, because most of the porosity in the bones of the adult horses was due to remodelling within the cortices, other reasons related to metabolic or growth processes may have played a role beyond the mechanical influences.

Most studies linking porosity and remodelling to mechanical strains engendered within vertebrate long bones have examined these relationships using exogenous loading regimes or perturbation conditions different from physiological loading. Increased remodelling rates were found in bone cortices subjected to either

increased strain magnitudes and/or strain frequencies (Burr et al. 1985; Bentolila et al. 1998; Lee et al. 2002; Lieberman et al. 2003), and are hypothesized to be the result of processes to repair microcracks within the bone cortex or from simply increasing bone strains above some critical physiological threshold (Lanyon et al. 1982; Burr et al. 1985; Lee et al. 2002). In such cases, the greatest amounts of remodelling would be expected to occur where the mechanical strains are greatest. However, if remodelling occurs as a result of metabolic or growth processes, it might be expected to occur where strains are lowest, so that removed bone material would least compromise the structural integrity of the bone.

In the goat radius, bone strains increased during ontogeny as porosity and remodelling decreased and increased, respectively. However, within each age/size group, regions of greater strain did not correspond to less porosity or greater remodelling, suggesting that these ontogenetic patterns of cortical modelling/remodelling may be related to physiological or mechanical influences unaccounted for here. A combination of the different possible factors regulating remodelling and porosity could produce the patterns observed here for the goat radius, in which the uniformly porous and highly vascularized bones of the younger goats are equally in-filled during ontogeny. This creates a less porous and stiffer support structure in the adult goats, whose bones are, in turn, remodelled in such a way that reflects more than just the mechanical influences, but potentially other biological processes as well. Without some sort of exogenous perturbational load, these processes (mechanical and biological) result in no correlation between the mechanical environment and the growth modelling and remodelling observed within the goat radius.

Although there was no significant correlation between remodelling and any of the measured mechanical variables, remodelling did correlate positively with the percentage of transverse collagen, which occurred in greatest abundance in the caudal region of the radius in all age groups. As peak strain magnitudes correlated positively with cortical thickness, the strains tended to be relatively low in this thin caudal region. Therefore, high locomotor strains were probably not responsible for the relatively greater remodelling in this location. The caudal region typically had the thinnest cortex in the radius with some of the lowest growth rates and was thus probably composed of some of the oldest bone material in the radius. As a result, despite the relatively low strains, this region might well accumulate fatigue damage over time, resulting in increased bone remodelling. However, there are two other features specific to the caudal region that could additionally influence remodelling within this part of the bone, the origins of the wrist and digital flexor muscles along this surface and the adjacent position of the ulna connected to this region (mostly subsection 8) by an interosseous ligament. Beyond affecting the mechanical environment along the bone's surface, the interaction between the bone and the fibrous insertions of these other features, over the course of growth, could potentially produce increased cortical remodelling in this caudal region.

Collagen fibre orientation and regional mechanical environments

The caudal region of the radius also showed a unique collagen fibre profile, having the highest percentage of transverse collagen, relative to other bone regions in all age groups. This pattern is consistent with previous studies for the horse radius, which also showed a high percentage of transverse or oblique collagen in the caudal region while the cranial region was primarily composed of longitudinal fibres (Boyde & Riggs, 1990; Riggs et al. 1993a; Mason et al. 1995). Results from mechanical tests have shown that bone enriched primarily with longitudinal collagen fibres is stronger in tension than bone composed primarily of transverse or oblique fibres, which is stronger in compression and shear, respectively (Evans & Vincentelli, 1969, 1974; Vincentelli & Evans, 1971). Consistent with this, mechanical tests of bone from the horse radius showed that the cranial surface is stronger in tension than compression and that the opposite is true for the caudal surface (Riggs et al. 1993b). Finally, strain gauge experiments found that the cranial surface of the horse radius is loaded maximally in tension and the caudal surface in compression (Turner et al. 1975; Rubin & Lanyon, 1982; Biewener et al. 1983). Taken as a whole, these studies indicate a close relationship between form and function in the horse radius with regards to collagen fibre orientation and regional strain patterns.

If strain gauges had only been attached to the cranial and caudal surfaces of the goat radius in the present study, as has generally been done previously for the horse radius, results linking fibre orientation and mechanical environment in the goat radius would have been consistent with those for the horse. However,

because the strain distributions in the goat radius were calculated for the entire mid-shaft cross-section over the entire stride period for the two younger groups, the results presented here attempting to link collagen fibre orientation with mechanical environment are inconsistent with previous work and in contrast to the hypothesized close relationship between fibre orientation and strain environment in the goat radius. Given the distribution of peaks strains in the radius (Table 3) and the positive correlation between strain magnitude and cortical thickness, it is clear that the greatest tensile and compressive strains generally occur in the lateral and medial regions of the bone, respectively. Although these regions of the radius showed very different peak strain magnitudes, they had very similar fibre orientations throughout ontogeny, being orientated predominantly in a longitudinal direction relative to the caudal region of the bone, which showed a higher percentage of transverse collagen, though not particularly high compressive strains. Thus, fibre orientation does not appear to relate well to the longitudinal strain environment in the goat radius.

It is possible, however, that regional collagen fibre orientations relate more closely to regional differences in other mechanical characteristics and not longitudinal strain patterns. However, results of the partial correlation tests showed (perhaps counter-intuitively) that the percentage of transverse collagen only had a significant (negative) relationship with the radial strain gradients, indicating that lower percentages of transverse collagen occurred where radial gradients were highest. This relationship was largely due to greater radial gradients in the thicker cortical subsections where peak strains were greater, but where the collagen fibres were orientated primarily longitudinally. The increased transverse (and oblique) collagen on the caudal surface also cannot be explained by higher shear strains in this region because in all three age groups the percentage of strain due to shear on this surface was not significantly different from the cranial surface ($P > 0.45$ for all paired *t*-test comparisons).

During preparation of the histological thin-sections, if the caudal region of the radius had been cut systematically thicker in all thin-sections, it would appear brighter under CPL and, thus, seemingly populated by more transverse collagen fibres (Boyde & Riggs, 1990). However, the thicknesses measured for the caudal regions of the thin-sections were not significantly greater than the other cortical regions ($P > 0.06$, $P > 0.26$ and $P > 0.33$ for all regional comparisons for the small, intermediate and adult groups, respectively). Similar to the trends observed for bone remodelling, the caudal region appears to be unique for some reason unrelated to the measured strain environments, but potentially related to growth and mechanical interactions associated with the ulna and/or muscle origins along this surface. Strong evidence in support of this would require that collagen fibres insert into this region, perpendicular to the bone's surface (Riggs et al. 1993a), to help anchor the interosseous ligament and/or the muscles. However, the transverse fibres in the caudal region of the bone, and the entire bone in general, tended to be orientated circumferentially in the primary bone and were associated specifically with the secondary osteons in the remodelled bone. Thus, it seems that the predominance of transverse collagen in the caudal region is probably not the result of muscle or fibrous insertions, although the possible effects of these neighbouring structures on the bone's histomorphology cannot be ignored.

Another interesting result was the pan-regional increase in transverse collagen in the adult goats. Undermineralized bone (Boyde & Riggs, 1990) or the bone of younger animals, which consists of more woven-fibred bone tissue (Riggs et al. 1993a) that is typically less well-mineralized (Currey & Pond, 1989; Brear et al. 1990), should appear brighter under CPL (Boyde & Riggs, 1990). The radii of the adult goats were more highly mineralized than those of the younger goats (Main & Biewener, 2004) and, given similar thin-section thicknesses and loading environments as the young goats, should have appeared uniformly darker. However, instead they appeared brighter. The increase in refracted light for the adult goats was not caused by greater sectional thicknesses for the adults (Boyde & Riggs, 1990), as these did not differ significantly from the two younger groups ($P > 0.77$ for all comparisons). These results for the adult goat radius, however, are similar to patterns reported for the human femur and turkey ulna, in which more highly mineralized bone and/or bone from older animals appeared brighter under CPL, suggesting a higher percentage of transverse collagen (Skedros et al. 2003; Goldman et al. 2005). More work investigating the effect of bone mineral content on CPL refraction is required before these results can be fully interpreted.

Another possible reason for the systematic brightness in the adult goat radii, indicating a higher percentage

of transverse collagen throughout the bone, could result from an overall different mechanical environment in the adult radius. A relative abundance of transverse or oblique collagen fibres should correlate with higher amounts of compressive axial or shear strain within mammalian long bones (Evans & Vincentelli, 1969, 1974). However, relative amounts of shear strain were not significantly different with age ($P > 0.26$ for all comparisons), and although not significant, there was a trend for a lower percentage of total strain due to axial compression ($P > 0.08$) in adult vs. younger goats. Thus, the greater brightness of the adult radii under CPL was not the result of greater axial or shear strains within their radii either.

Because the distribution of longitudinal strains for the adult goats were not measured through the entire stance phase (Biewener & Taylor, 1986), it is not known for certain what types of strains all bone cortices of the adult radius experienced. This makes it difficult to completely discount the mechanical environment as a reason for why the adult goat bones appeared brighter under CPL. As in many previous studies attempting to link mechanical environment to histomorphometry without obtaining both bone strain measurements and histological data from the same animals, the specific mechanical environment for the bones examined remains unknown, limiting interpretations of remodelling patterns to a more speculative nature.

Conclusions

The mechanical environment in the goat radius is not fixed over the course of a stride. Rotation of the neutral axis during stance causes all regions of the bone's cortex to experience both tension and compression. Although some cortices experience significantly greater longitudinal strain rates and radial gradients, and/or significantly more longitudinal compression or tension than others, the difference is not enough to elicit strong histomorphometric differences in the cortex, assuming that bone histology should reflect the mechanical forces on the bone in some way. It is possible that the regional histological patterns in the goat radius do match the measured strain environments, but because strain environments were variable during stance, showing few distinct regional differences, the histomorphology also shows few regional differences. Additionally, these experiments only accounted for bone strains produced during steady treadmill locomotion, whereas the histomorphology would also be affected by the activities of these animals in their paddocks, which may produce more variable loading within the limb.

However, two histomorphological characters do clearly differ among the various bone subsections: higher growth rates and thicker cortices in the medial and lateral regions and a relatively high percentage of transverse collagen in the caudal region. The thicker cortices and higher growth rates in the medial and lateral regions of the bone are significant because, within an age group, it seems likely that they contribute structurally to help maintain relatively uniform strain ranges and general peak strain magnitudes in these regions. Although these regions of the radius were generally loaded under higher peak compressive and tensile strains, respectively, the magnitudes were not usually significantly different from the strains experienced by the thinner neighbouring subsections.

Collagen fibre orientation also differed significantly between certain subsections but was not correlated with either mechanical environment or measured growth patterns. The unique orientation of the collagen fibres in the caudal region of the radius could result from the adjacent position of the ulna and/or the origination of the wrist and digital flexor muscles along this surface. However, as with most of the histological variables examined here, other factors must be considered as well, such as the surrounding anatomy, inherent growth patterns and metabolism, which could certainly affect the bones' histomorphology.

Although few correlations between growth patterns, histomorphometry and strain environment were found here for the goat radius during ontogeny, perhaps with a larger sample size, detailed strain data from an entire (not partial) ontogenetic series, and even a stronger regionalization of strain patterns within the bone, possible correlations between histomorphometry and mechanical environment in vertebrate long bones might be revealed.

Acknowledgements

I thank Andy Biewener for his advice and support of this work, Pedro Ramirez for animal care, many members of the Concord Field Station for assistance during data collection, Joyce Main for assistance with data analysis, and Craig McGowan and Ty Hedrick for advice

and assistance with the Matlab programs. Andrew Lee provided advice and instruction regarding the CPL technique. Dan Lieberman kindly let me use his microscope and visual fluorescence equipment, and Maureen Devlin provided microscopy assistance and advice. Earlier drafts of this paper were improved by comments from Andy Biewener, Dan Lieberman and two anonymous reviewers. This work was supported in part by the Chapman Fund (Harvard University).

References

Beaupré GS, Orr TE, Carter DR (1990) An approach for time-dependent bone modeling and remodeling – theoretical development. *J Orthopaedic Res* **8**, 651–661.

Bentolila V, Boyce TM, Fyhrie DP, Drumb R, Skerry TM, Schaffler MB (1998) Intracortical remodeling in adult rat long bones after fatigue loading. *Bone* **23**, 275–281.

Bertram JEA, Biewener AA (1988) Bone curvature: sacrificing bone strength for load predictability? *J Theoret Biol* **131**, 75–92.

Bertram JEA, Swartz SM (1991) The 'Law of Bone Transformation': a case of crying Wolff. *Biol Rev* **66**, 245–273.

Biewener AA, Thomason J, Lanyon LE (1983) Mechanics of locomotion in the forelimb of the horse (*Equus*): in vivo stress developed in the radius and metacarpus. *J Zool Lond* **201**, 67–82.

Biewener AA, Taylor CR (1986) Bone strain: a determinant of gait and speed? *J Exp Biol* **123**, 383–400.

Biewener AA (1991) Musculoskeletal design in relation to body size. *J Biomechanics* **24**, 19–29.

Biewener AA (1992) *In vivo* measurement of bone strain and tendon force. In *Biomechanics- Structures and Systems* (ed. Biewener AA), pp. 123–147. New York: Oxford University Press.

Biewener AA, Dial KP (1995) *In vivo* strain in the humerus of pigeons (*Columba livia*) during flight. *J Morph* **225**, 61–75.

Biewener AA, Fazzalari NL, Konieczynski DD, Baudinette RV (1996) Adaptive changes in trabecular architecture in relation to functional strain patterns and disuse. *Bone* **19**, 1–8.

Blob RW, Biewener AA (1999) *In vivo* locomotor strain in the hindlimb bones of *Alligator mississippiensis* and *Iguana iguana*: implications for the evolution of limb bone safety factor and non-sprawling limb posture. *J Exp Biol* **202**, 1023–1046.

Boyde A, Riggs CM (1990) The quantitative study of the orientation of collagen in compact bone slices. *Bone* **11**, 35–39.

Brear K, Currey JD, Pond CM (1990) Ontogenetic changes in the mechanical properties of the femur of the polar bear *Ursus maritimus*. *J Zool Lond* **222**, 49–58.

Bromage TG, Goldman HM, McFarlin SC, Warshaw J, Boyde A, Riggs CM (2003) Circularly polarized light standards for investigations of collagen fiber orientation in bone. *Anat Rec Part B: New Anat* **274B**, 157–168.

Burr DB, Martin RB, Schaffler MB, Radin EL (1985) Bone remodeling in response to *in vivo* fatigue microdamage. *J Biomechanics* **18**, 189–200.

Burr DB, Robling AG, Turner CH (2002) Effects of biomechanical stress on bones in animals. *Bone* **30**, 781–786.

Carrier D (1983) Postnatal ontogeny of the musculo-skeletal system in the Black-tailed jack rabbit (*Lepus californicus*). *J Zool Lond* **201**, 27–55.

Carter DR, Orr TE, Fyhrie DP (1989) Relationships between loading history and femoral cancellous bone architecture. *J Biomechanics* **22**, 231–244.

Currey JD, Pond CM (1989) Mechanical properties of very young bone in the axis deer (*Axis axis*) and humans. *J Zool Lond* **218**, 59–67.

Currey JD (2002) *Bones: Structures and Mechanics*. Princeton, NJ: Princeton University Press.

Demes B, Stern JT Jr, Hausman MR, Larson SG, McLeod KJ, Rubin CT (1998) Patterns of strain in the macaque ulna during functional activity. *Am J Phys Anthropol* **106**, 87–100.

Demes B, Qin Y, Stern JT Jr, Larson SG, Rubin CT (2001) Patterns of strain in the macaque tibia during functional activity. *Am J Phys Anthropol* **116**, 257–265.

Dytham C (2003) *Choosing and Using Statistics: a Biologist's Guide*. Oxford: Blackwell Publishing.

Evans FG, Vincentelli R (1969) Relation of collagen fiber orientation to some mechanical properties of human cortical bone. *J Biomechanics* **2**, 63–71.

Evans FG, Vincentelli R (1974) Relations of the compressive properties of human cortical bone to histological structure and calcification. *J Biomechanics* **7**, 1–10.

Francillon-Vieillot H, de Buffrénil V, Castanet J, et al (1990) Microstructure and mineralization of vertebrate skeletal tissues. In *Skeletal Biomineralization: Patterns, Processes, and Evolutionary Trends*, Vol. 1 (ed. Carter JG), pp. 471–548. New York: Van Nostrand Reinhold.

Frost HM (1983) A determinant of bone architecture: the minimum effective strain. *Clin Orthopaedics Related Res* **175**, 286–292.

Goldman HM, Thomas CDL, Clement JG, Bromage TG (2005) Relationships among microstructural properties of bone at the human midshaft femur. *J Anat* **206**, 127–139.

Goodship AE, Lanyon LE, McFie H (1979) Functional adaptation of bone to increased stress – experimental study. *J Bone Joint Surg Am* **61**, 539–546.

Gross TS, McLeod KJ, Rubin CT (1992) Characterizing bone strain distributions *in vivo* using three triple rosette strain gauges. *J Biomechanics* **25**, 1081–1087.

Gross TS, Edwards JL, McLeod KJ, Rubin CT (1997) Strain gradients correlate with sites of periosteal bone formation. *J Bone Miner Res* **12**, 982–988.

Horner JR, de Ricqlès A, Padian K (2000) Long bone histology of the hadrosaurid dinosaur *Maiasaura peeblesorum*: growth dynamics and physiology based on an ontogenetic series of skeletal elements. *J Vertebrate Paleontol* **20**, 115–129.

Hsieh Y, Robling AG, Ambrosius WT, Burr DB, Turner CH (2001) Mechanical loading of diaphyseal bone in vivo: the strain threshold for an osteogenic response varies with location. *J Bone Miner Res* **16**, 2291–2297.

Judex S, Gross TS, Zernicke RF (1997) Strain gradients correlate with sites of exercise-induced bone-forming surfaces in the adult skeleton. *J Bone Miner Res* **12**, 1737–1745.

Judex S, Zernicke RF (2000) Does the mechanical milieu associated with high-speed running lead to adaptive changes in diaphyseal growing bone. *Bone* **26**, 153–159.

Lanyon LE, Goodship AE, Pye CJ, MacFie JH (1982) Mechanically adaptive bone remodeling. *J Biomechanics* **15**, 141–154.

Lanyon L (1987) Functional strain in bone tissue as an objective, and controlling stimulus for adaptive bone remodelling. *J Biomechanics* **20**, 1083–1093.

Lee AH (2004) Histological organization and its relationship to function in the femur of *Alligator mississippiensis*. *J Anat* **204**, 197–207.

Lee KCL, Lanyon LE (2004) Mechanical loading influences bone mass through estrogen receptor α. *Exercise Sport Sci Rev* **32**, 64–68.

Lee TC, Staines A, Taylor D (2002) Bone adaptation to load: microdamage as a stimulus for bone remodeling. *J Anat* **201**, 437–446.

Lieberman DE, Pearson OM, Polk JD, Demes B, Crompton AW (2003) Optimization of bone growth and remodeling in response to loading in tapered mammalian limbs. *J Exp Biol* **206**, 3125–3138.

Lieberman DE, Polk JD, Demes B (2004) Predicting long bone loading from cross-sectional geometry. *Am J Phys Anthropol* **123**, 156–171.

Main RP, Biewener AA (2004) Ontogenetic patterns of limb loading. *In vivo* bone strains and growth in the goat radius. *J Exp Biol* **207**, 2577–2588.

de Margerie E (2002) Laminar bone as an adaptation to torsional loads in flapping flight. *J Anat* **201**, 521–526.

de Margerie E, Sanchez S, Cubo J, Castanet J (2005) Torsional resistance as a principal component of the structural design of long bones: comparative multivariate evidence in birds. *Anat Rec Part A* **282A**, 49–66.

Martin RB (2002) Is all cortical bone remodeling initiated by microdamage? *Bone* **30**, 8–13.

Martin RB, Burr DB, Sharkey NA (1998) *Skeletal Tissue Mechanics*. New York: Springer.

Mason MW, Skedros JG, Bloebaum RD (1995) Evidence of strain-mode-related cortical adaptation in the diaphysis of the horse radius. *Bone* **17**, 229–237.

McMahon JM, Boyde A, Bromage TG (1995) Pattern of collagen fiber orientation in the ovine calcaneal shaft and its relation to locomotor-induced strain. *Anat Rec* **242**, 147–158.

van der Meulen MCH, Beaupré GS, Carter DR (1993) Mechanobiologic influences in long bone cross-sectional growth. *Bone* **14**, 635–642.

Mosley JR, March BM, Lynch J, Lanyon LE (1997) Strain magnitude related changes in whole bone architecture in growing rats. *Bone* **20**, 191–198.

Mosley JR, Lanyon LE (1998) Strain rate as a controlling influence on adaptive modeling in response to dynamic loading of the ulna in growing male rats. *Bone* **23**, 313–318.

Mosley JR, Lanyon LE (2002) Growth rate rather than gender determines the size of the adaptive response of the growing skeleton to mechanical strain. *Bone* **30**, 314–319.

Parfitt AM (2002) Targeted and nontargeted bone remodeling: relationship to basic multicellular unit origination and progression. *Bone* **30**, 5–7.

Pauwels F (1980) *Biomechanics of the Locomotor Apparatus*. New York: Springer.

Pearson OM, Lieberman DE (2004) The aging of Wolff's 'Law': ontogeny and responses to mechanical loading in cortical bone. *Yearb Phys Anthropol* **47**, 63–99

Pontzer H, Lieberman DE, Momin E, et al (2006) Trabecular bone in the bird knee responds with high sensitivity to changes in load orientation. *J Exp Biol* **209**, 57–65.

Riggs CM, Lanyon LE, Boyde A (1993a) Functional associations between collagen fibre orientation and locomotor strain direction in cortical bone of the equine radius. *Anat Embryol* **187**, 231–238.

Riggs CM, Vaughan LC, Evans GP, Lanyon LE, Boyde A (1993b) Mechanical implications of collagen fibre orientation in cortical bone of the equine radius. *Anat Embryol* **187**, 239–248.

Robling AG, Duijvelaar KM, Geevers JV, Ohashi N, Turner CH (2001) Modulation of appositional and longitudinal bone growth in the rat ulna by applied static and dynamic force. *Bone* **29**, 105–113.

Rubin CT, Lanyon LE (1982) Limb mechanics as a function of speed and gait: a study of functional strains in the radius and tibia of horse and dog. *J Exp Biol* **101**, 187–211.

Rubin CT, Lanyon LE (1985) Regulation of bone mass by mechanical strain magnitude. *Calcified Tissue Int* **37**, 411–417.

Rubin C, Gross T, Qin Y, Fritton S, Guilak F, Mcleod K (1996) Differentiation of the bone-tissue remodeling response to axial and torsional loading in the turkey ulna. *J Bone Joint Surg* **78-A**, 1523–1533.

Skedros JG, Bloebaum RD, Mason MW, Bramble DM (1994) Analysis of a tension/compression skeletal system: possible strain-specific differences in the hierarchical organization of bone. *Anat Rec* **239**, 396–404.

Skedros JG, Hunt KJ, Hughes PE, Winet H (2003) Ontogenetic and regional morphologic variations in the turkey ulna diaphysis: implications for functional adaptation of cortical bone. *Anat Rec Part A* **273A**, 609–629.

Thomas CDL, Feik SA, Clement JG (2005) Regional variation of intracortical porosity in the midshaft of the human femur: age and sex differences. *J Anat* **206**, 115–125.

Turner AS, Mills EJ, Gabel AA (1975) *In vivo* measurement of bone strain in the horse. *Am J Vet Res* **36**, 1573–1579.

Vico L, Collet P, Guignandon A, et al (2000) Effects of long-term microgravity exposure on cancellous and cortical weight-bearing bones of cosmonauts. *Lancet* **355**, 1607–1611.

Vincentelli R, Evans FG (1971) Relations among mechanical properties, collagen fibers, and calcification in adult human cortical bone. *J Biomechanics* **4**, 193–201.

Wolff J (1892) *The Law of Bone Remodeling*. Berlin: Springer.